

Supporting information for

**Enhanced compatibility of a polymer-based electrolyte with Li-metal for stable and
dendrite-free all-solid-state Li-metal batteries**

Hasan Jamal¹, Firoz Khan², Hyeong-Rok Si¹ and Jae Hyun Kim^{1*}

¹Division of Energy Technology, Daegu Gyeongbuk Institute of Science & Technology, 333,
Techno Jungang-Daero, Hyeonpung-Myeon, Dalseong-Gun, Daegu 42988, Republic of
Korea.

²Interdisciplinary Research Center for Renewable Energy and Power Systems (IRC-REPS),
Research Institute, King Fahd University of Petroleum & Minerals (KFUPM), Dhahran-
31261, Saudi Arabia

*Correspondence: jaehyun@dgist.ac.kr; Tel.: +82-53-7853610; Fax: +82-53-7853439

Fabrication of LiFePO₄ (LFP) and LiNiCoAlO₂ (NCA) cathodes

The slurry for the LFP cathode was synthesized using 90 wt.% LFP powder, 5 wt.% super P, and 5 wt.% polyvinylidene fluoride (PVDF). These ingredients were dissolved in N-Methyl-2-pyrrolidone (NMP) and properly mixed them using high energy ball-milling. The cathode was coated on the Al-foil using doctor blade technique. Then the coated samples were dried in vacuum at 110 °C for 12 h. The charge-discharge characterization was carried out using the CR2032 type coin cell. The Li-foil was acted as an anode and reference electrode. The specific capacity was calculated using active mass of cathode. For the NCA cathode, a similar procedure was followed. The current densities at 1C are 170 and 195 mA g⁻¹ are used for LFP and NCA cathodes, respectively.

Degree of crystallinity calculation from DSC data

DSC data were acquired for phase transition behavior of the YNa-CPE with Li-salt contents of 10% to 40% including glass transition temperature (T_g), melting temperature (T_m), enthalpy of melting (ΔH_m) and degree of crystallinity (X_c). The degree of crystallinity (X_c) is calculated using Eq. (S1),

$$x_c \equiv \frac{\Delta H_m}{\Delta H_0} \quad (S1)$$

where, ΔH_m was obtained from DSC results, and ΔH_0 is the melting enthalpy of 100% crystalline PEO (213.7 J/g).^{1,2}

Activation energy calculation

The Vogel-Tamman-Fulcher (VTF) Eq. (S2) is used to determine the value of activation energy (E_a) of YNa-CPEs.³

$$\sigma = AT^{-1/2} e^{\frac{-E_a}{R(T - T_0)}} \quad (\text{S2})$$

Where, A = pre-exponential element, T = temperature, R = universal gas constant (0.008314 kJ mol⁻¹ K⁻¹, and T₀ = equilibrium glass-transition temperature of the copolymer (T₀ = T_g - 50).

The eq. (S2) can be arranged as

$$\log(\sigma \cdot T^{1/2}) = \log(A) - \frac{E_a}{R(T - T_0)} \quad (\text{S3})$$

The curves between $\log(\sigma \cdot T^{1/2})$ vs. $\frac{1}{(T - T_0)}$ were plotted for each sample as shown in Fig.S14.

Moreover, the curves were linearly fitted. The slope of the curve with the $\frac{1}{(T - T_0)}$ axis

provides the value of E_a, whereas the intercept on the $\log(\sigma \cdot T^{1/2})$ axis gives the value of A.

The obtained values of E_a and log(A) are listed in [Table S5](#).

Table S1. Composition of PEO, LiTFSI, and ZYNa dispersed in ACN (15 mL) for the synthesis of YNa-CPE. Ball milling time for all the samples is 48 h.

Sample names	PEO (g)	LiTFSI (g)	ZYNa (g)
10%	0.40	0.04	0.0251
20%	0.40	0.08	0.0251
30%	0.40	0.12	0.0251
35%	0.40	0.14	0.0251
40%	0.40	0.16	0.0251

Table S2. Crystallographic data and Rietveld refinement results of ZYNa by powder XRD data: atomic coordinates, site occupancies, isotropic displacement parameters and reliability factors at room temperature.

Crystal System	Cubic					
Space Group	F d -3 m (no. 227)					
Lattice Parameter, Volume, Z	$a = 24.644(1) \text{ \AA}$, $V = 14967(2) \text{ \AA}^3$, $Z = 32$					
Atoms	x	y	z	Wyckoff	Occupancy	U_{iso} 100
Si1	-0.0536(2)	0.1226(4)	0.0363(3)	192 <i>i</i>	0.6094	9.5(4)
Al1	-0.0536(2)	0.1226(4)	0.0363(3)	192 <i>i</i>	0.3906	9.5(4)
O1	-0.1051(2)	0.0000	0.1051(2)	96 <i>h</i>	1.0000	9.5(4)
O2	-0.0008(2)	-0.0008(2)	0.1421(3)	96 <i>g</i>	1.0000	9.5(4)
O3	-0.0323(2)	0.0725(4)	0.072(4)	96 <i>g</i>	1.0000	9.5(4)
O4	0.0716(2)	0.0716(2)	0.3190(3)	96 <i>g</i>	1.0000	9.5(4)
Na1	0.0000	0.0000	0.0000	16 <i>c</i>	0.1250	9.5(4)
Na2	0.0515(2)	0.0515(2)	0.0515(2)	32 <i>e</i>	0.8750	9.5(4)
Na3	0.2320(2)	0.2320(2)	0.2320(2)	32 <i>e</i>	1.0000	9.5(4)
Na4	0.1037(2)	0.1462(2)	0.3924(3)	96 <i>e</i>	0.0521	9.5(4)
Na5	0.0654(2)	0.0654(2)	0.4040(3)	96 <i>e</i>	0.0521	9.5(4)

Table S3. DSC data for phase transition behavior of YNa-CPEs including the values of T_g , T_m , Change of T_m , Heat capacity, ΔH_m , and X_c .

Sample names	T_g ($^{\circ}$ C)	T_m ($^{\circ}$ C)	Change of T_m (%)	Heat capacity ($J/g^{\circ}C$)	ΔH_m (J/g)	X_c (%)
10%	-47.97	63.56	0	16.06	132.16	61.84
20%	-48.37	59.42	6.51	9.60	95.79	44.82
30%	-48.62	55.33	12.94	5.64	66.91	31.31
35%	-48.97	50.78	20.10	4.99	53.79	25.14
40%	-49.21	46.35	27.07	3.67	37.72	17.65

Table S4. Ionic conductivities of YNa-CPEs, measured at various temperatures (20, 30, 40, 50, 60, and 70 °C).

Li-salt contents (wt%)	σ (S/cm)					
	20 °C	30 °C	40 °C	50 °C	60 °C	70 °C
10	7.20×10^{-6}	1.65×10^{-5}	3.25×10^{-5}	9.33×10^{-5}	1.77×10^{-4}	2.71×10^{-4}
20	2.36×10^{-5}	6.55×10^{-5}	1.62×10^{-4}	4.09×10^{-4}	7.04×10^{-4}	1.00×10^{-3}
30	1.03×10^{-4}	5.33×10^{-4}	2.06×10^{-3}	4.71×10^{-3}	8.18×10^{-3}	1.06×10^{-2}
35	1.32×10^{-4}	6.56×10^{-4}	2.82×10^{-3}	1.10×10^{-2}	1.66×10^{-2}	2.39×10^{-2}
40	7.69×10^{-5}	4.73×10^{-4}	2.63×10^{-3}	7.89×10^{-3}	1.13×10^{-2}	1.62×10^{-2}

Table S5. The fitting parameter to obtain the activation energy of the YNa-CPEs.

Li-salt contents (wt%)	Slop [E _a /R] (K)	Intercept [log(A)]	E _a (kJ/mol)
10	-276.49	0.055	2.2987
20	-234.48	0.257	1.9494
30	-215.36	1.126	1.7905
35	-205.24	1.37	1.7063
40	-191.96	1.082	1.5959

Table S6. Analyzed parameter values used for the determination of t_{Li^+} at 60 °C.

Sample	I_0 (μA)	I_s (μA)	R_0 (Ω)	R_s (Ω)	ΔV (mV)	t_{Li^+}
10%	14.3	6.2	393.24	411.32	10	0.54
20%	15.9	11.8	312.17	386.61	10	0.76
30%	23.5	17.3	337.20	355.88	10	0.81
35%	27.2	21.0	325.93	346.36	10	0.84
40%	21.1	16.1	274.88	291.24	10	0.82

Table S7. Comparison of electrochemical performance of composite polymer electrolytes-based Li-metal solid-state batteries.

Electrolyte	σ (S/cm)	Cathode/Anode	WV (V)	WT (°C)	SC (mAh/g)	RR (%) (after cycles) C rate	t_{Li^+}	LW (mg/cm ²)	Ref.
PEO-LiTFSI-HMOP*	4.0×10^{-4} @65 °C	LiFPO ₄ /Li	2.9-3.8	65	131	91.6 (100) 0.5 C	NA	2	4
PEO-LiTFSI-SSZ-13	4.4×10^{-5} @20 °C 1.91×10^{-3} @60 °C	LiFPO ₄ /Li	2.8-4.0	58	169	92 (160) 0.1 C	0.5	4.0	5
PEO-LiTFSI-M-SSZ-13	6.16×10^{-4} @30 °C 5.34×10^{-2} @ 70 °C	LiFPO ₄ /Li	2.6-4.3	60	154	94.0 (80) 0.1 C	0.85	2.2	6
PEO-LiTFSI-LAGP-SN	1.26×10^{-4} @30 °C	LiFPO ₄ /Li	2.8-3.8	40	152	91.2 (200) 0.1 C	0.50	2~3	7
PEO-LiTFSI-LLTO** nanowires	5.53×10^{-5} @ rt 3.63×10^{-4} @ 60 °C	LiFPO ₄ /Li	3.0-3.8	60	127	94.0 (100) 0.5 C	0.19	NA	8
PEO-LiPF ₆ -MOF [¶]	4.7×10^{-4} @ 30 °C	LiFPO ₄ /Li	2.5-4.0	25	115	69.56 (300) 1.0 C	0.68	4~5	9
PEO-LiTFSI – LLZO ^{\$} nano wires	2.39×10^{-4} @25 °C 1.53×10^{-3} @ 60 °C	LiFPO ₄ /Li	2.8-4.2	60	178	91.7 (120) 0.1 C	NA	1.68	10
PEO-LiTFSI – LLZTO ^{\$} particles	1.17×10^{-4} @30 °C	LiFPO ₄ /Li	2.6-4.0	55	127	93.6 (100) 0.2 C	NA	2~3	11
PEO-LiTFSI-ZYNa	6.56×10^{-4} @30 °C 2.39×10^{-2} @ 60 °C	LiFPO ₄ /Li	2.6-4.0	60	156	95.0 (100) 0.1 C	0.84	2.2~2.5	This work

WV = working voltage, WT = working temperature, SC = specific capacity, RR = retention rate, t_{Li^+} = Li-ion transference number and LW = loading weight

* HMOP = Hollow mesoporous organic polymer

** LLTO = $Li_{0.33}La_{0.557}TiO_3$

¶ MOF = Metal-organic framework

^{\$}LLZO = $Li_7La_3Zr_2O_{12}$

^{\$}LLZTO = $Li_{6.4}La_3Zr_{1.4}Ta_{0.6}O_{12}$

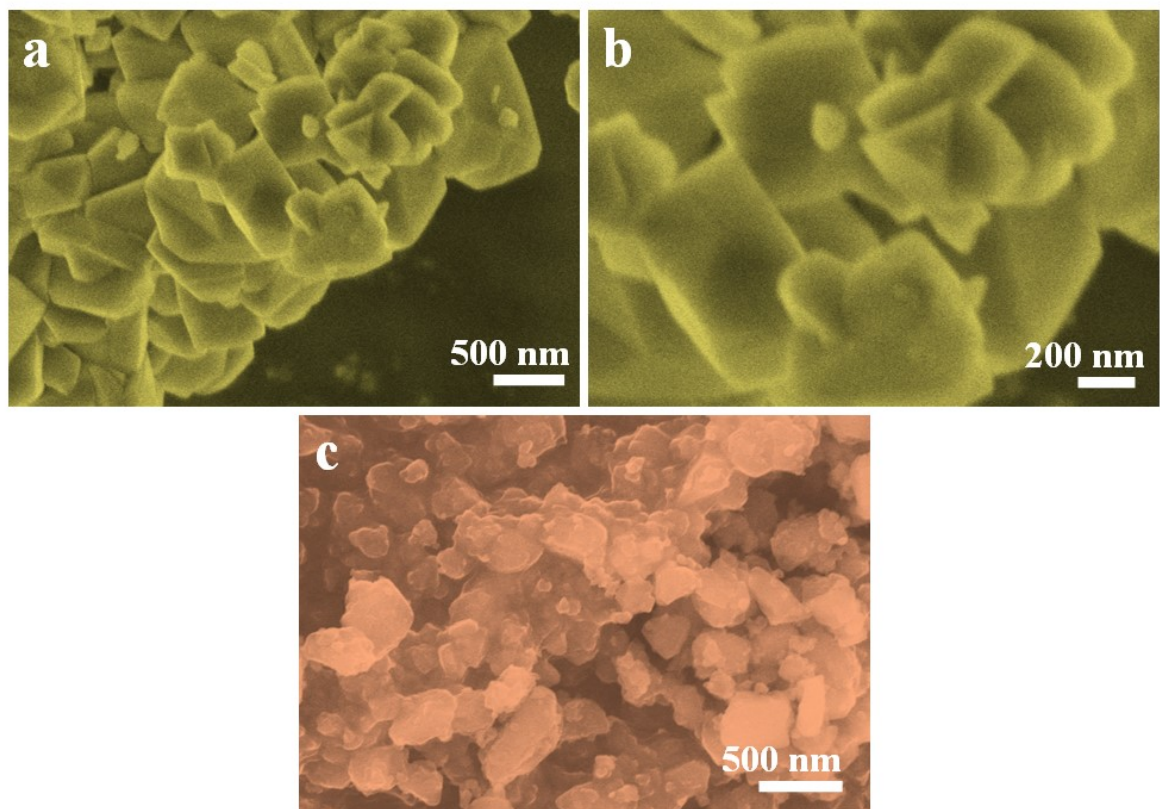


Fig. S1. The SEM images of (a, b) pristine ZYNa at different scale and (c) ZYNa after 48 h ball mill.

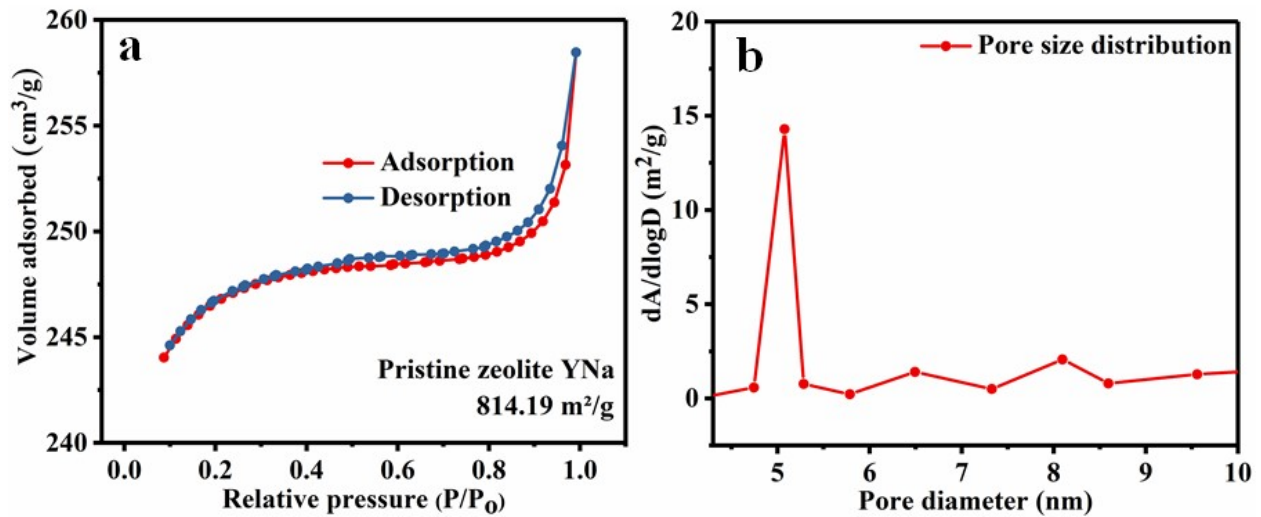


Fig. S2. Nitrogen adsorption-desorption isotherm of (a) pristine ZYNa and (b) BJH pore size distribution curve of ZYNa.

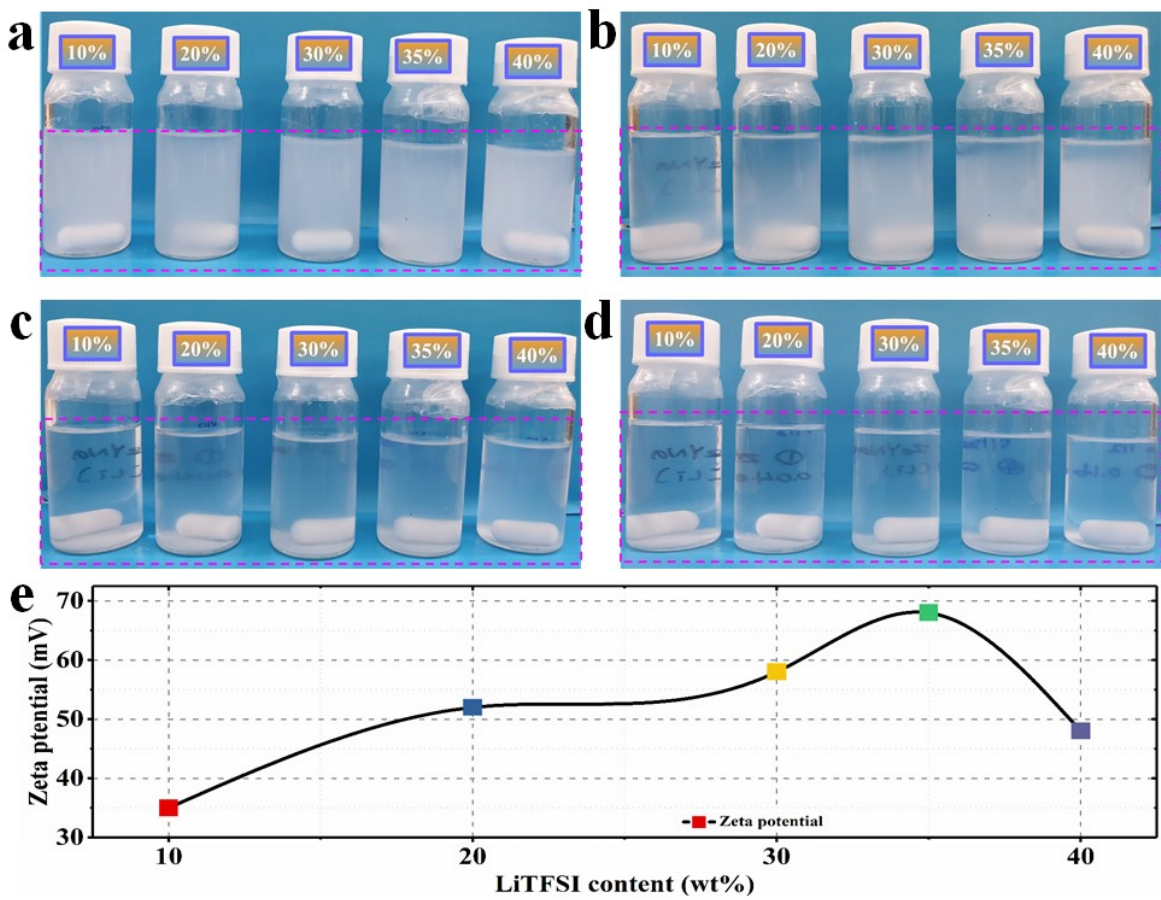


Fig. S3. Dispersion of ZYNa and LiTFSI in acetonitrile solvent. Optical image of ZYNa dispersed colloidal solution of (a) just after 24 h stirring, (b) dispersion stability after 5 min, (c) dispersion stability after 20 min, (d) dispersion stability after 1 h, and (e) zeta potential of ZYNa measured in acetonitrile for different Li-salt content.

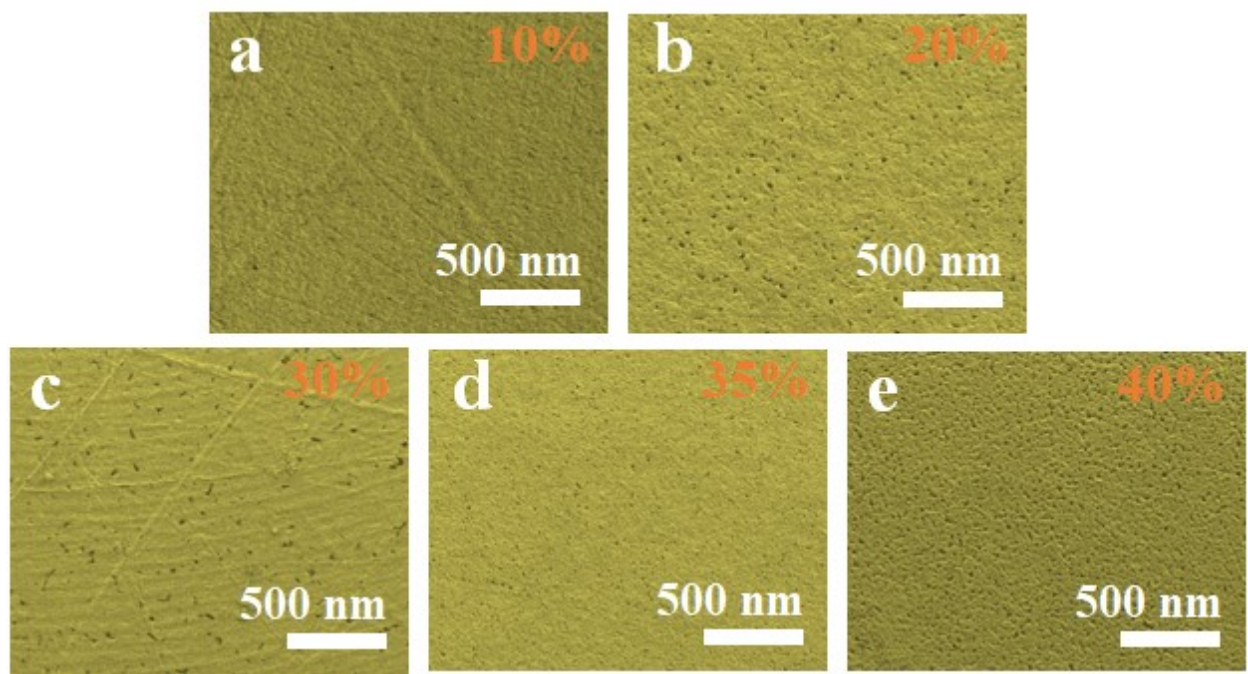


Fig. S4. The SEM images of YNa-CPEs for (a) YNa-CPE-10, (b) YNa-CPE-20, (c) YNa-CPE-30, (d) YNa-CPE-35, and (e) YNa-CPE-40.

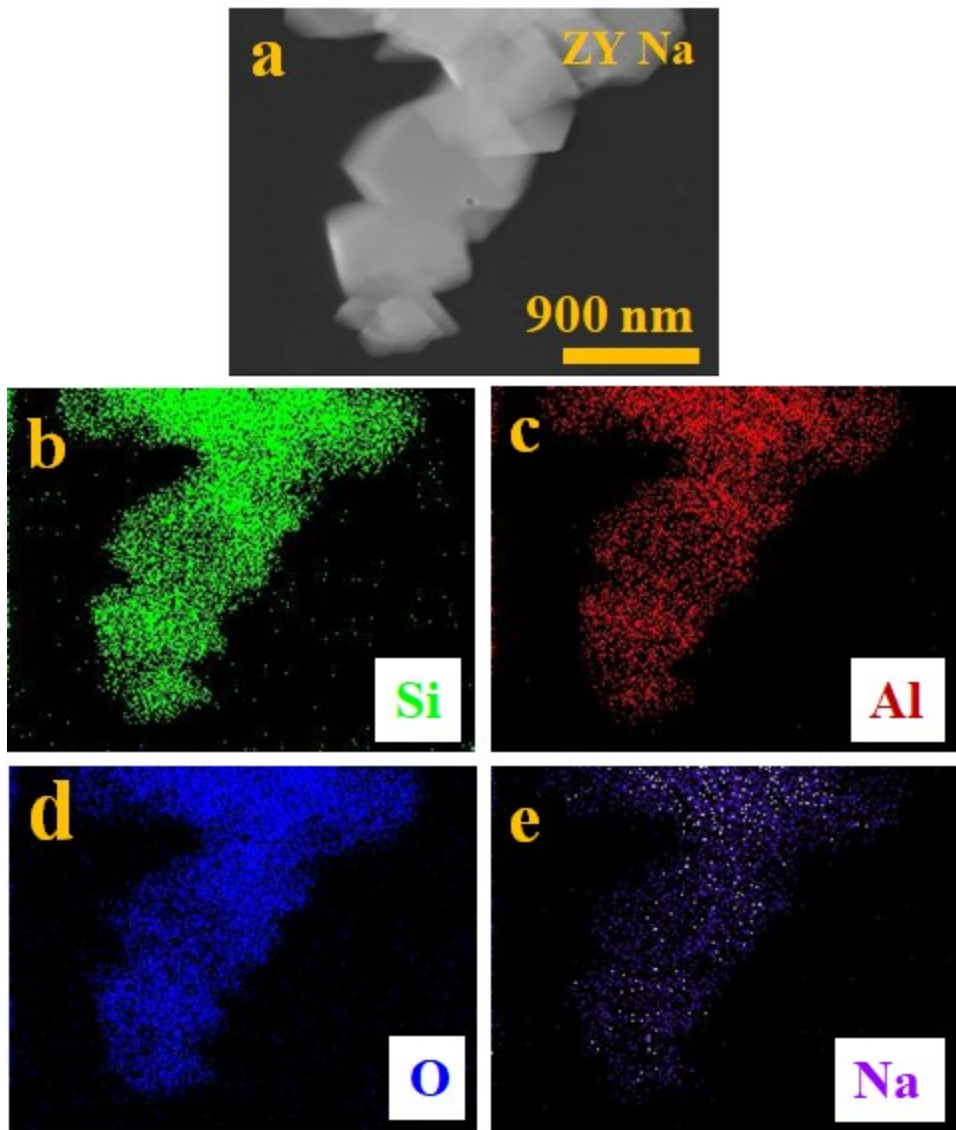


Fig. S5. The TEM image and TEM-EDS mapping of pristine ZYNa (a) TEM image. EDS mapping of (b) Si, (c) Al, (d) O, and (e) Na elements.



Fig. S6. The optical images of YNa-CPEs with different Li-salt content of (a) 10%, (b) 20%, (c) 30%, (d) 35%, and (e) 40%. Illustration of the flexibility and bendability of YNa-CPE-35 (f) before bending, (g) bending at different angles, and (h) returned to initial state after bending.

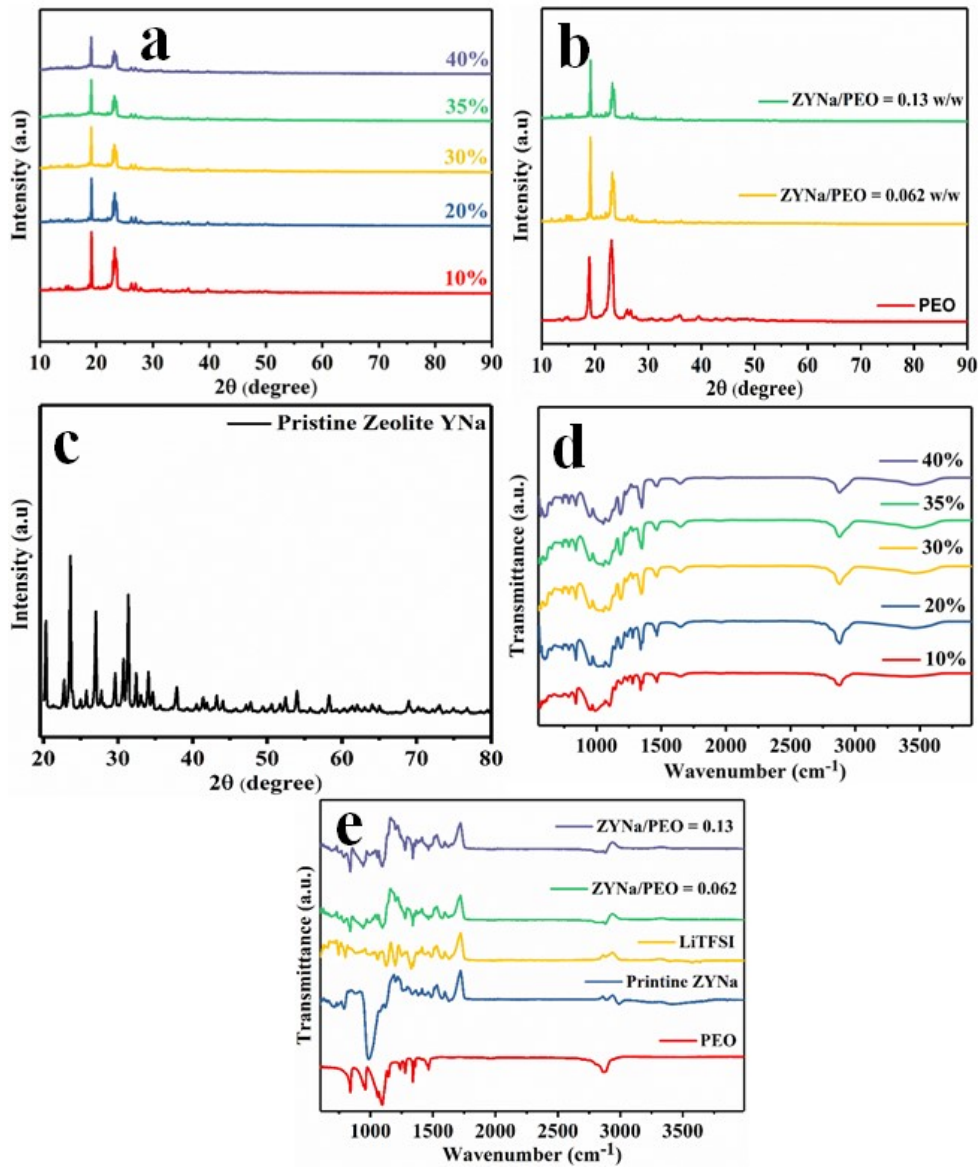


Fig. S7. The XRD patterns of (a) YNa-CPEs, (b) PEO, ZYNa/PEO = 0.062 w/w and ZYNa/PEO = 0.13 w/w, (c) pristine Zeolite YNa. FTIR spectra of (d) YNa-CPEs, and (e) PEO, pristine YNa, LiTFSI, ZYNa/PEO = 0.062 w/w and ZYNa/PEO = 0.13.

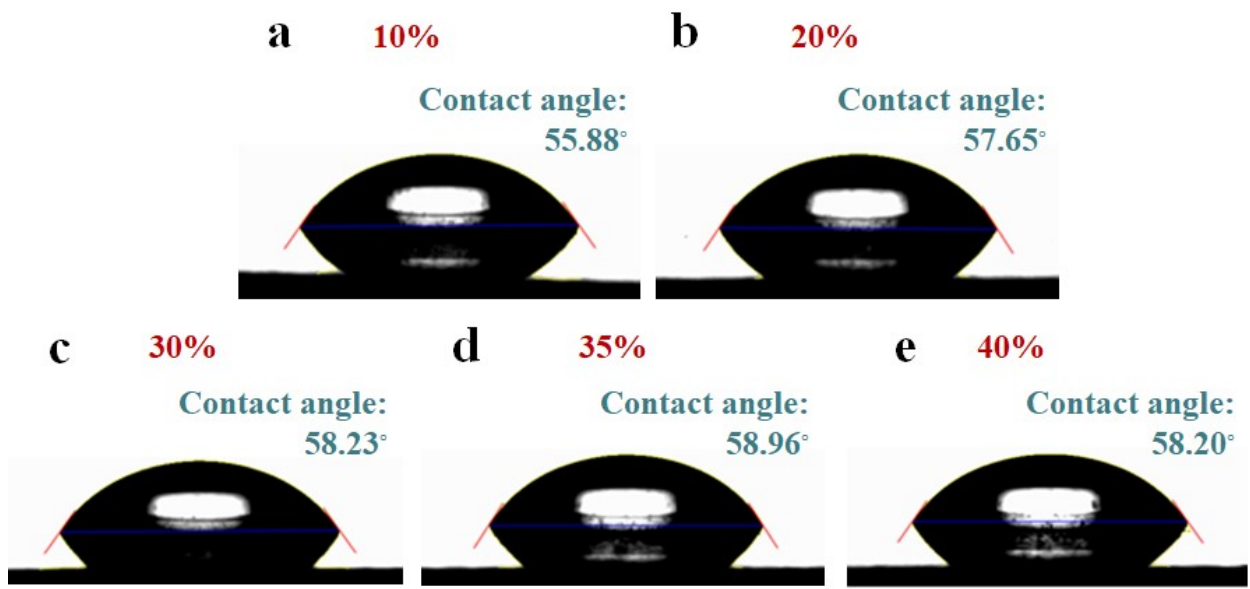


Fig. S8. The contact angle images of YNa-CPEs were obtained after coating the sample on the Si wafer for L-salt contents of (a) 10% (b) 20% (c) 30% (d) 35%, and (e) 40%.

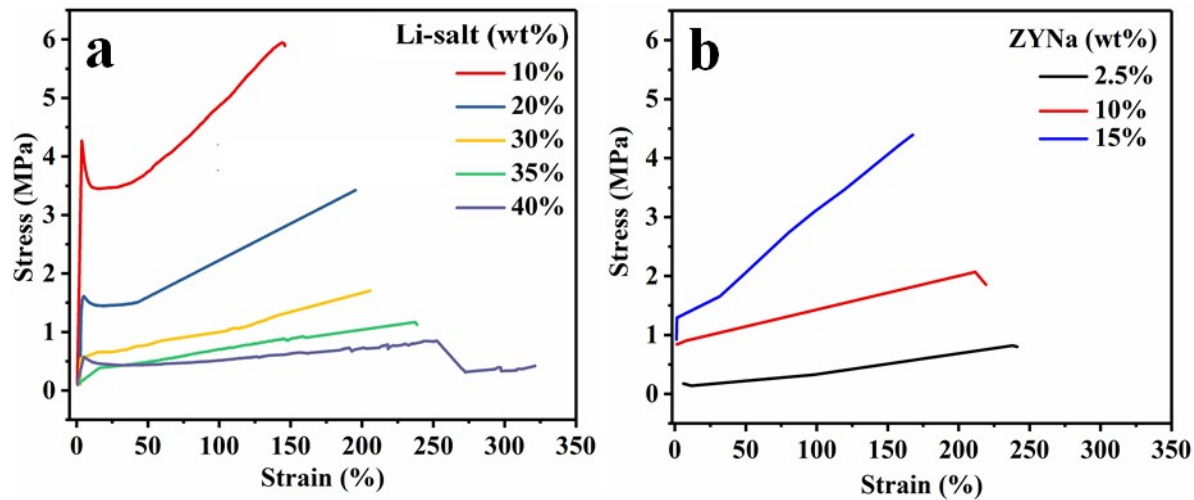


Fig. S9. Stress-strain curves of YNa-CPE for various (a) Li-salt contents (10% to 40%) and (b) ZYNa wt% of 2.5%, 10%, and 15% at room temperature (scan rate = 10 mm s⁻¹).

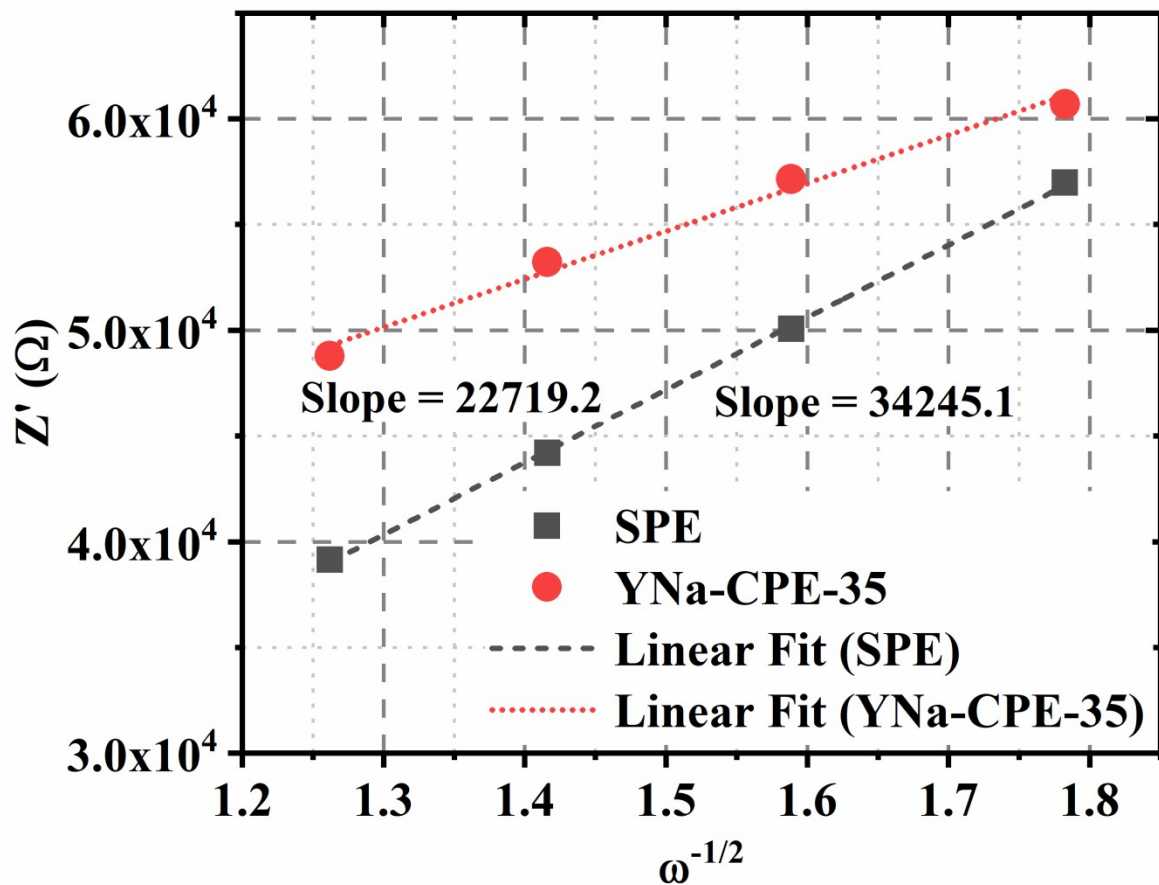


Fig. S10. Warburg coefficient determination from the low-frequency region of EIS curves for pristine SPE and YNa-CPE-35.

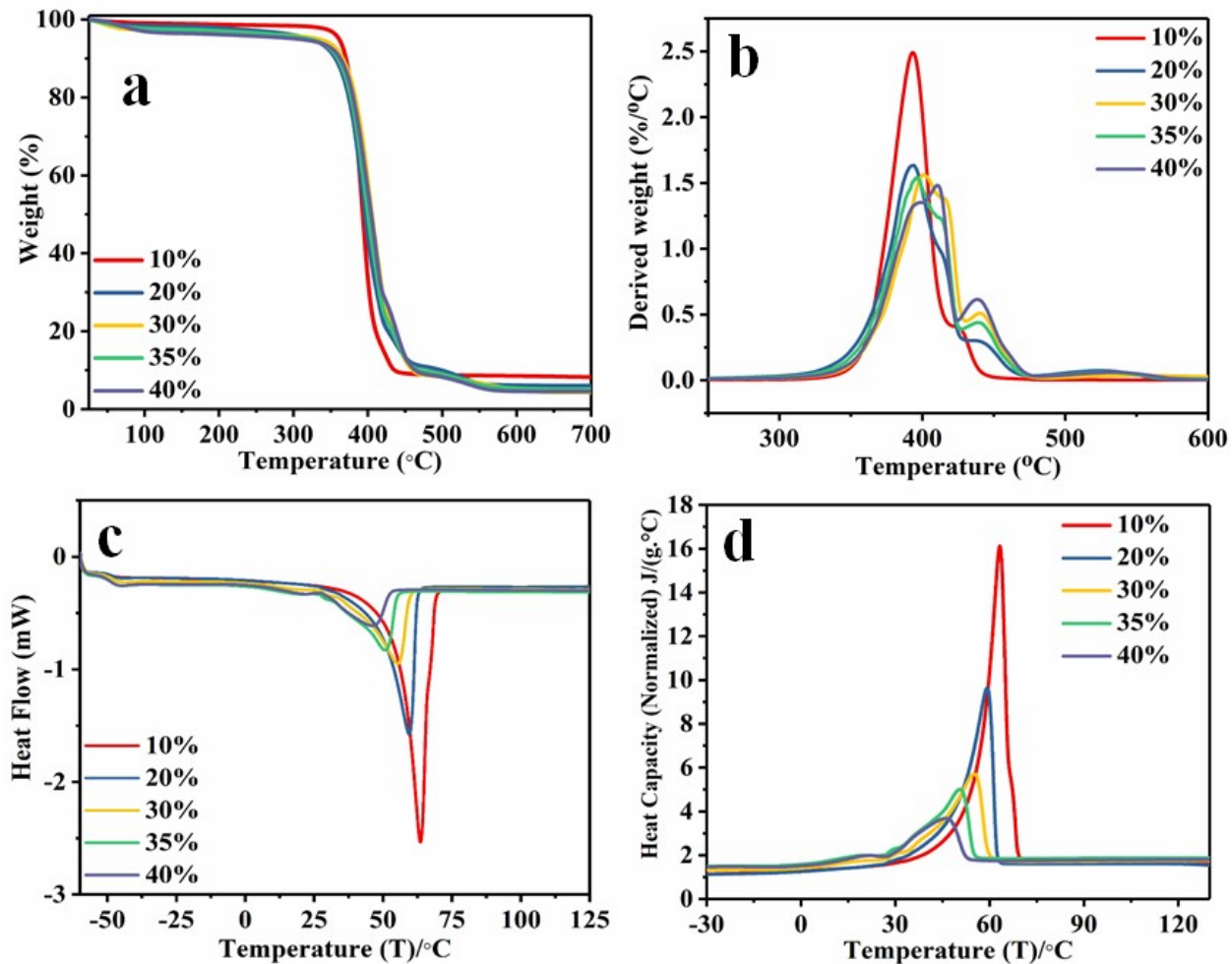


Fig. S11. (a) TGA curves in the temperature range of 40 – 700 °C, (b) derived weight vs. temperature curves in the temperature range of 250 – 600 °C, (c) DSC curves from -40 °C to 125 °C at a rate of 10 °C min⁻¹ (under N₂ flow), and (d) heat capacity (normalized, J g⁻¹ °C) vs temperature (T)/°C in the temperature range of -30 to 130 °C of YNa-CPEs.

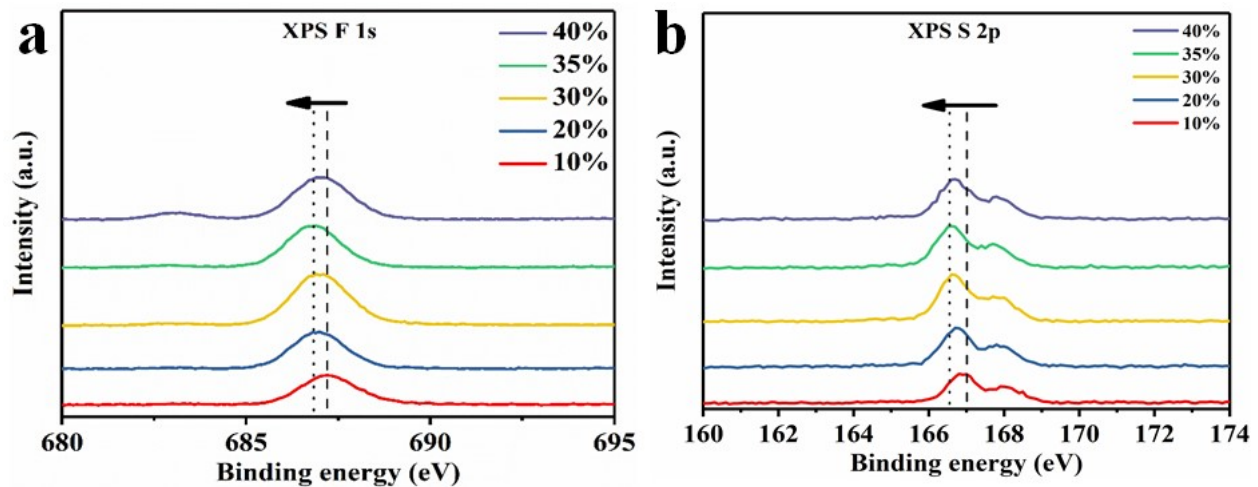


Fig. S12. XPS spectra of YNa-CPEs of (a) F 1s and (b) S 2p scan before cycling.

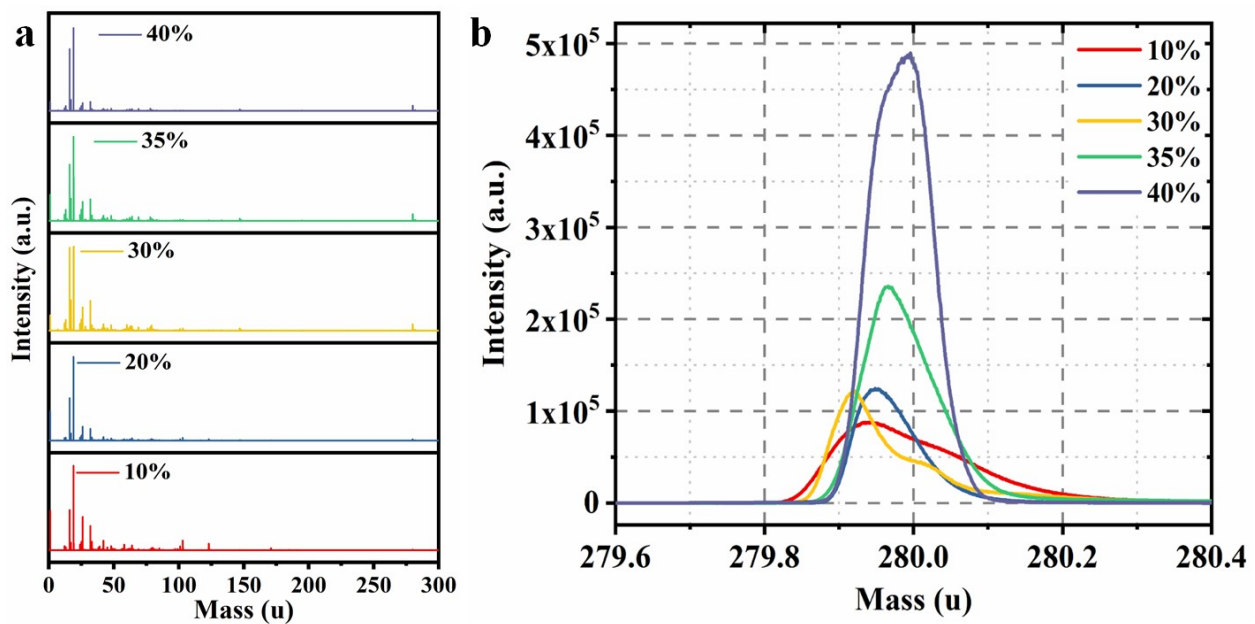
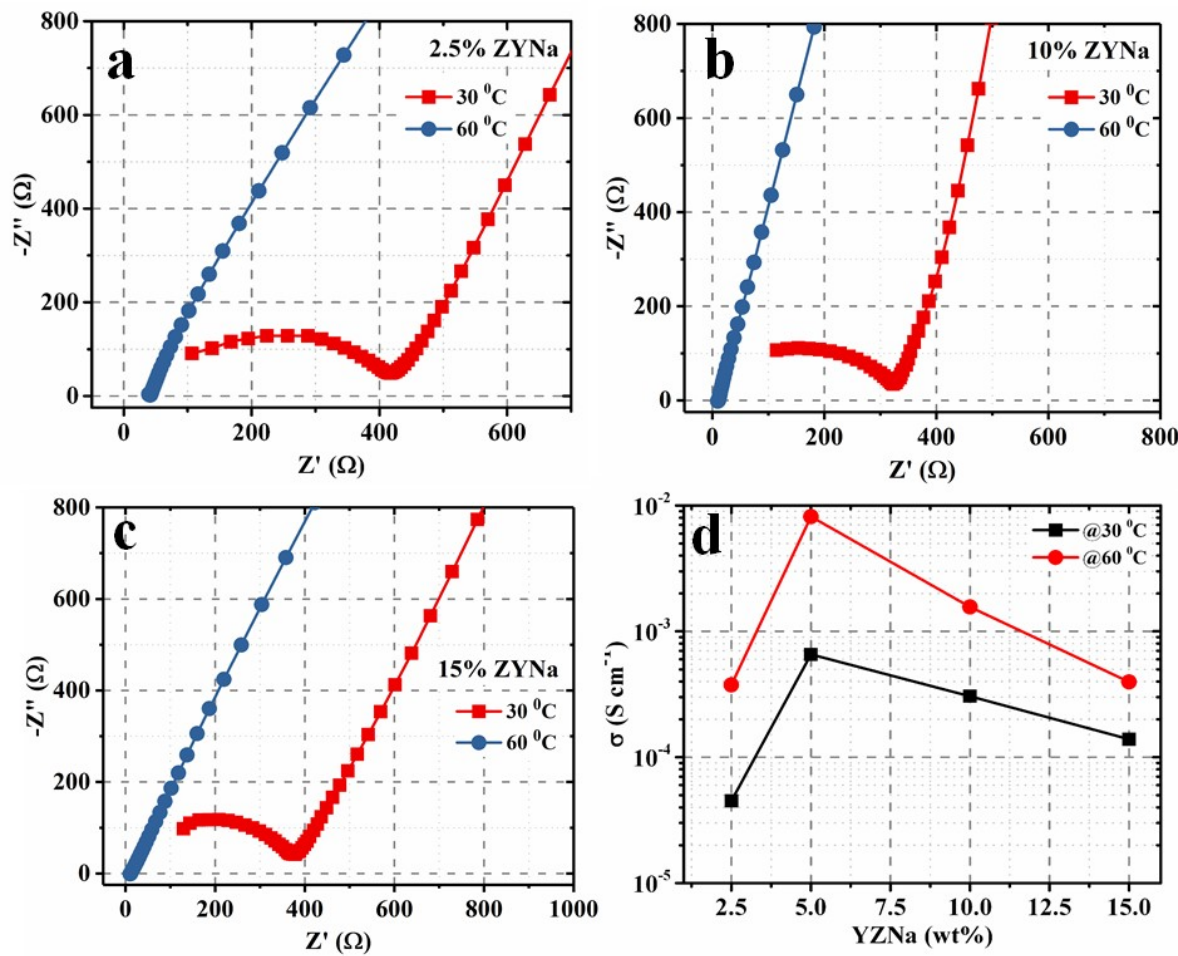


Fig. S13. TOF-SIMS spectrum of negative ions of the YNa-CPEs in the mass unit range of (a) 0 – 300 u and (b) 279.6 – 280.4 u before cycling.



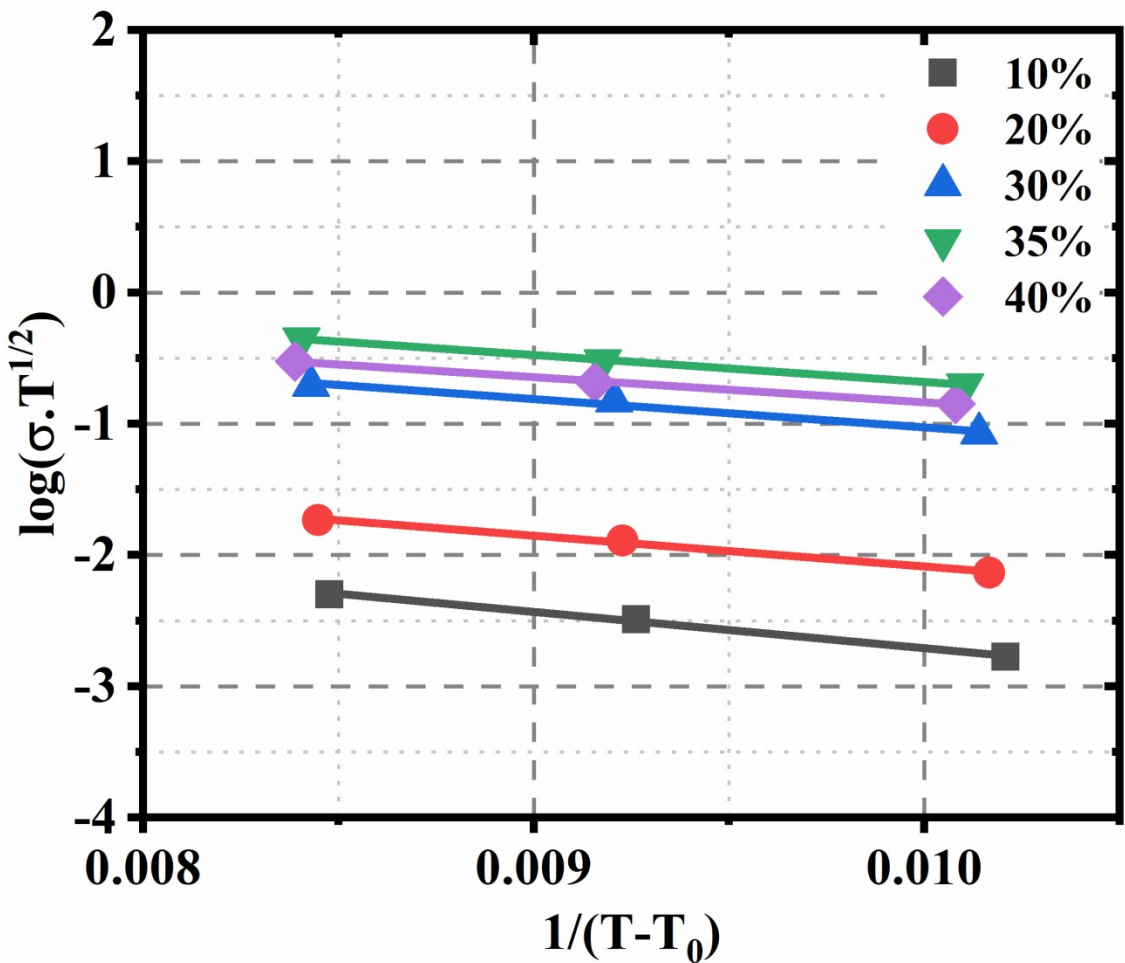


Fig. S15. VTF fitting results [between $\log(\sigma \cdot T^{1/2})$ vs. $\frac{1}{(T - T_0)}$] for determination of the activation energy of YNa-CPEs.

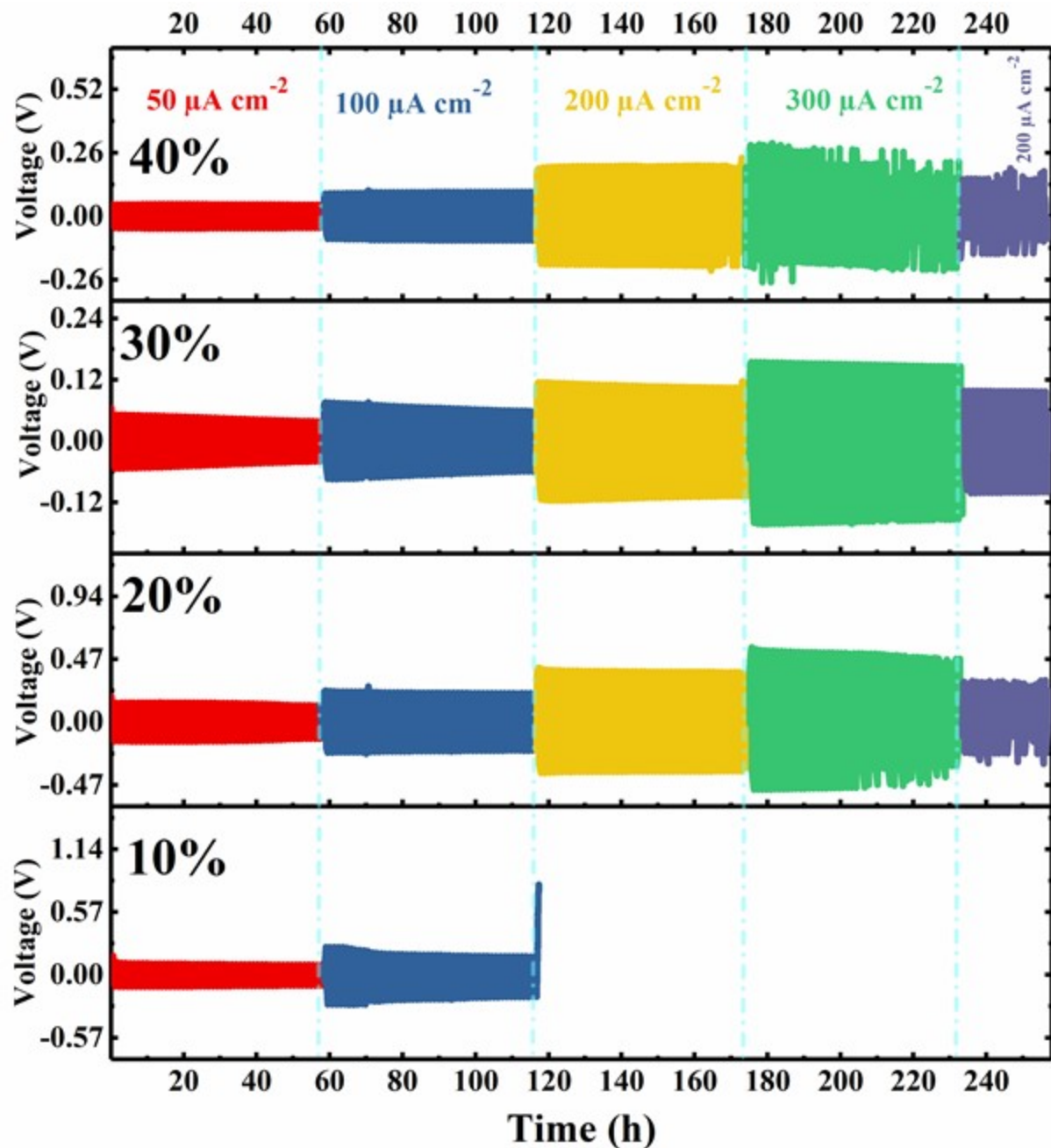


Fig. S16. Cyclic performance of YNa-CPEs for various Li-salt contents (10%, 20%, 30%, and 40%) using coin cell $[\text{Li}|\text{YNa-CPE}|\text{Li}]$ at current densities of 50, 100, 200 and 300 $\mu\text{A cm}^{-2}$ @60 $^{\circ}\text{C}$.

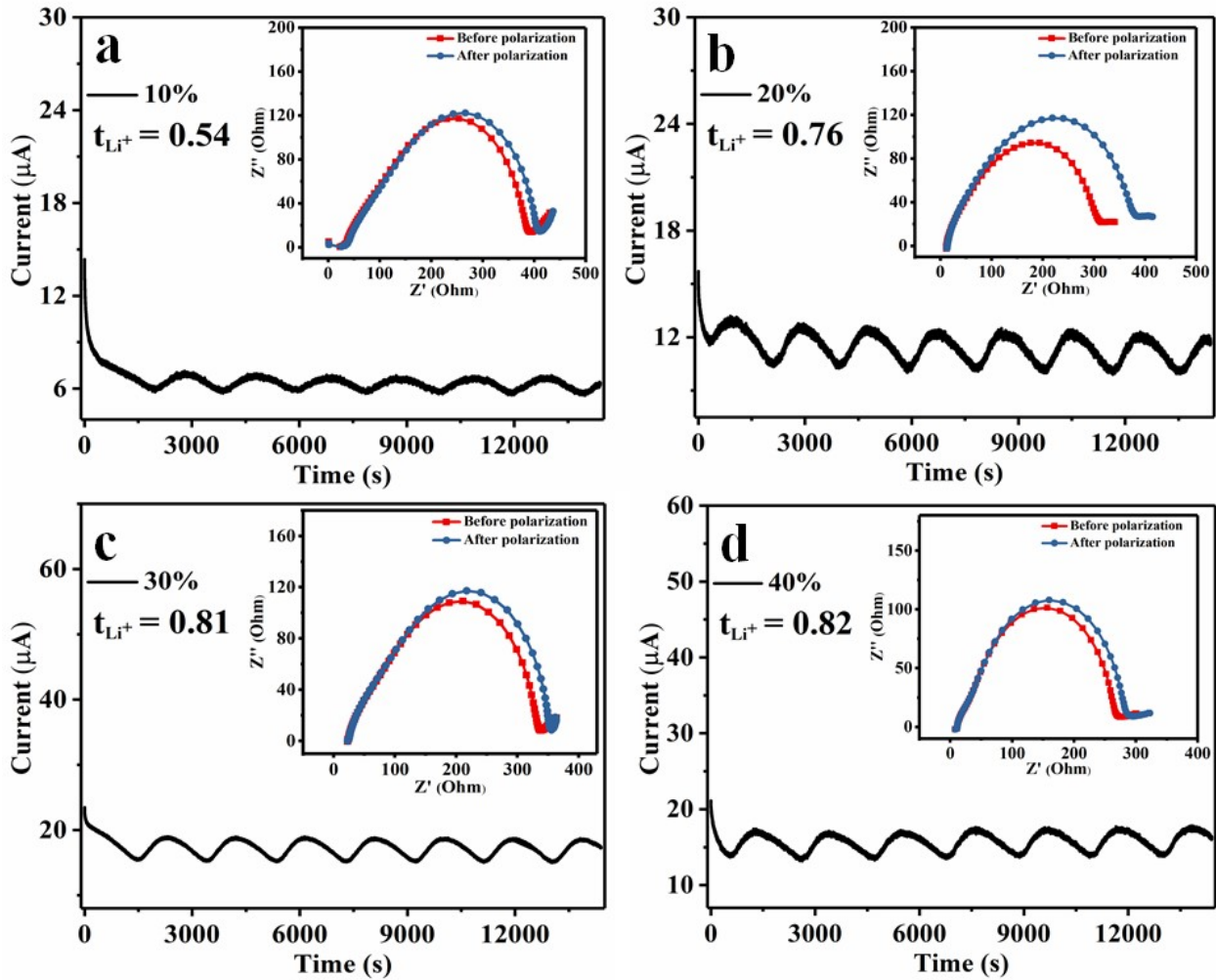


Fig. S17. Current-time profile for YNa-CPEs for Li-salt content of (a) 10%, (b) 20%, (c) 30%, and (d) 40% of coin cell [Li|YNaCPE|Li] @60 °C with polarization voltage of 10 mV for 4 h (inset: the EIS before and after polarization).

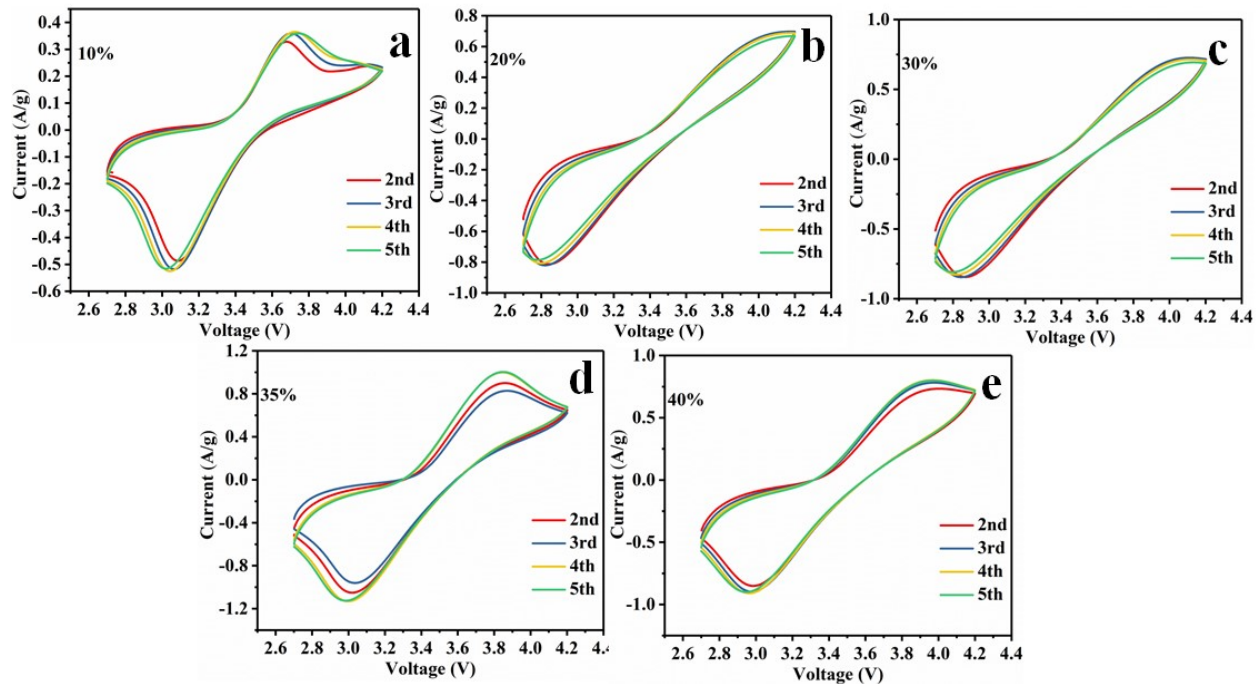
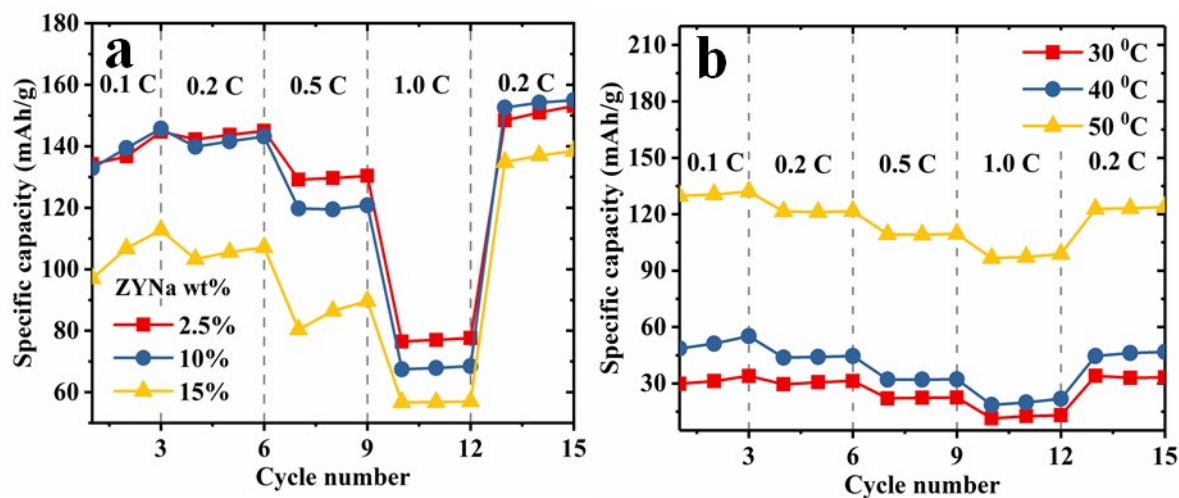


Fig. S18. Cyclic voltammogram of YNa-CPEs with different Li-salt contents of (a) 10%, (b) 20%, (c) 30%, (d) 35%, and (e) 40% using the [Li|YNa-CPE |LFP] coin cell at a sweep rate of 10 mV s^{-1} @ 60°C from 2nd to 5th cycles.



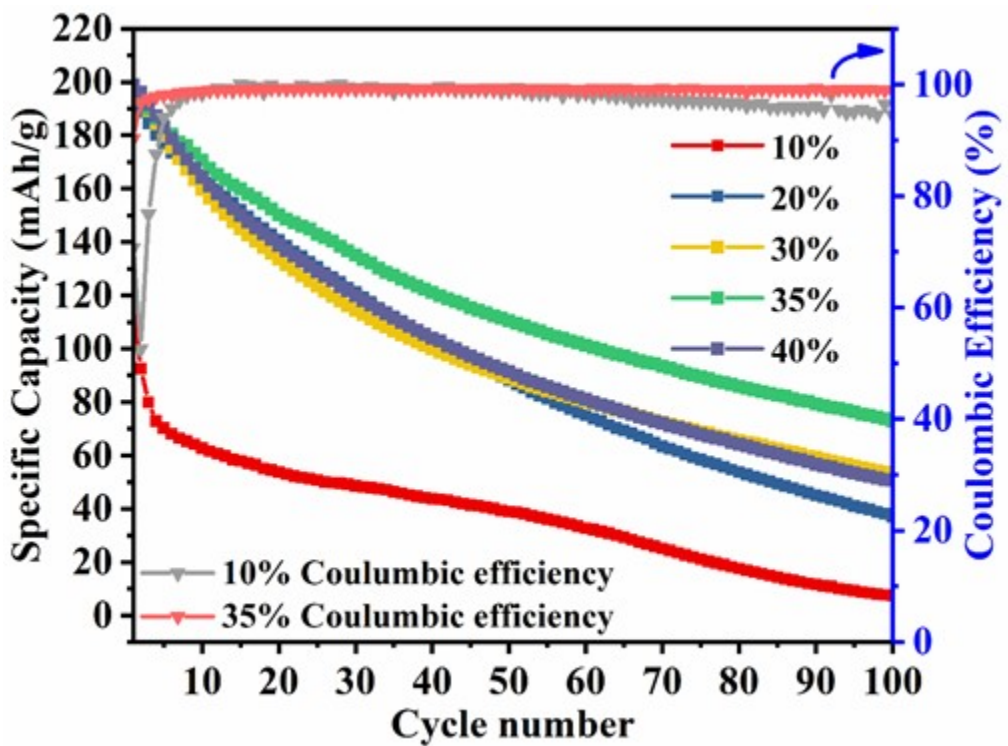


Fig. S20. Cycling performance of YNa-CPEs and columbic efficiency for Li-salt content of 10% and 35% using [Li|YNa-CPE|NCA] cell structure for 100 cycles at a C-rate of 0.1C @60 °C.

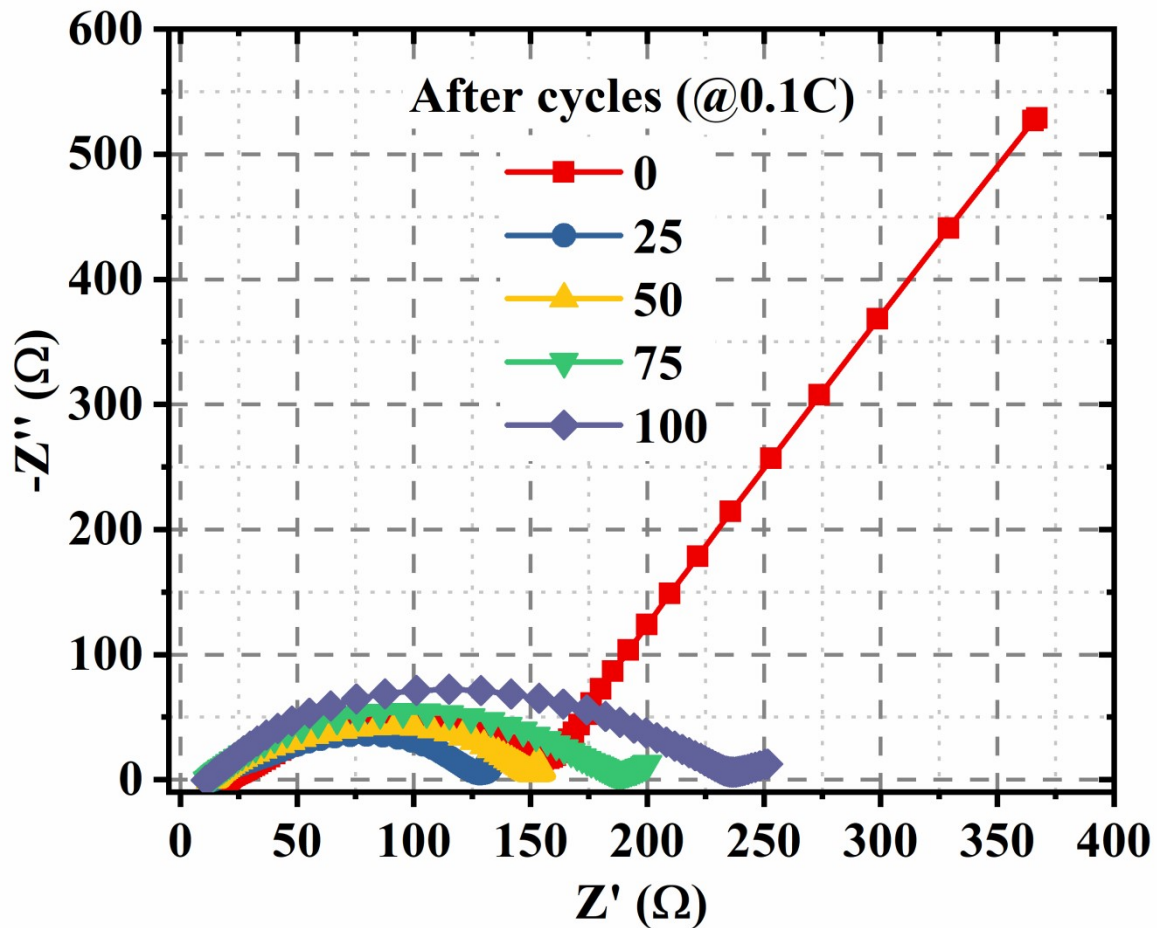


Fig. S21. EIS spectra during cycling of [Li|YNa-CPE-35|LFP] cell after various cycles (0 – 100) at @60 °C.

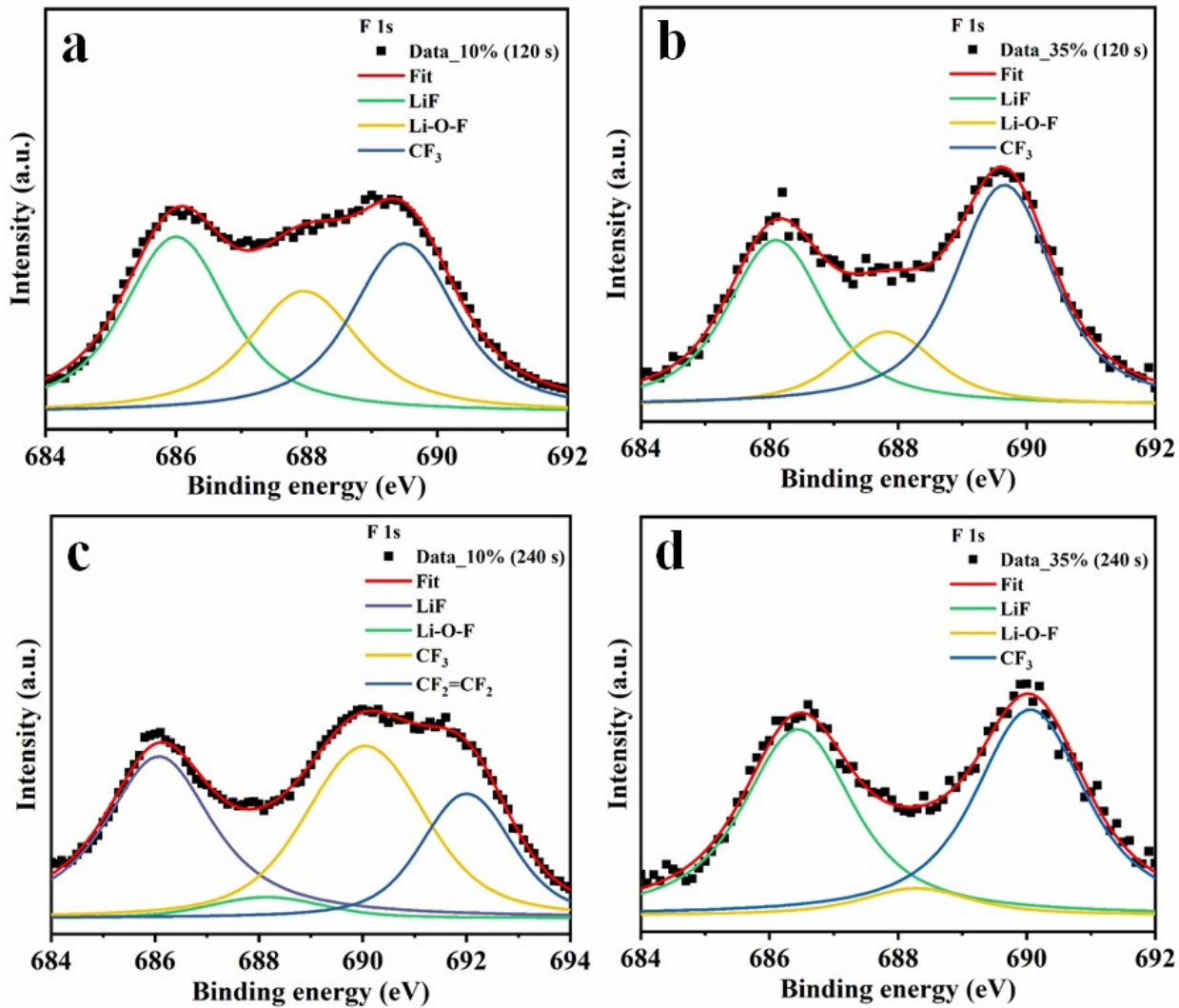


Fig. S22. Fitted XPS spectra of cycled YNa-CPEs (10% and 35%) for (a) F 1s scan after etching time of 120 s for 10%, (b) after etching time of 120 s for 35%, (c) after etching time of 240 s for 10%, and (d) after etching time of 240 s for 35% using [Li|YNa-CPE|LFP] cell structure along Li-side.

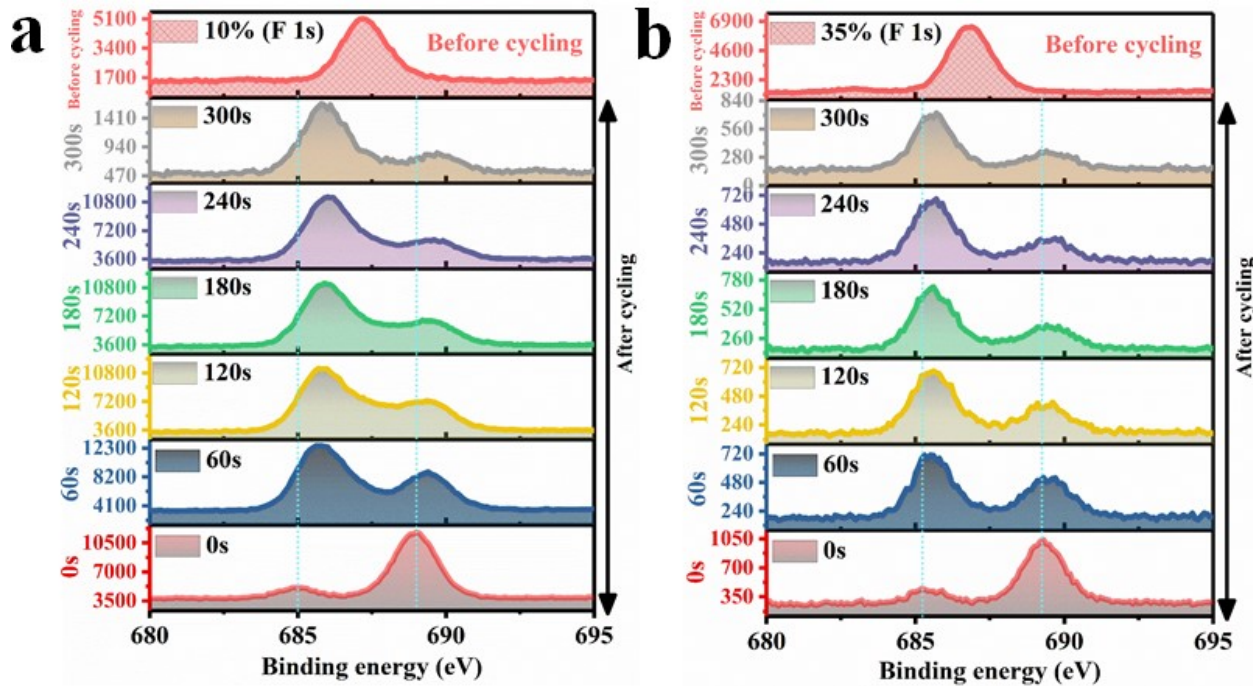


Fig. S23. XPS spectra for F1s scan of (a) YNa-CPE-10, and (b) ZYNa-CPE-35 before and after cycling along LFP-side for the etching time of 0 – 300 s.

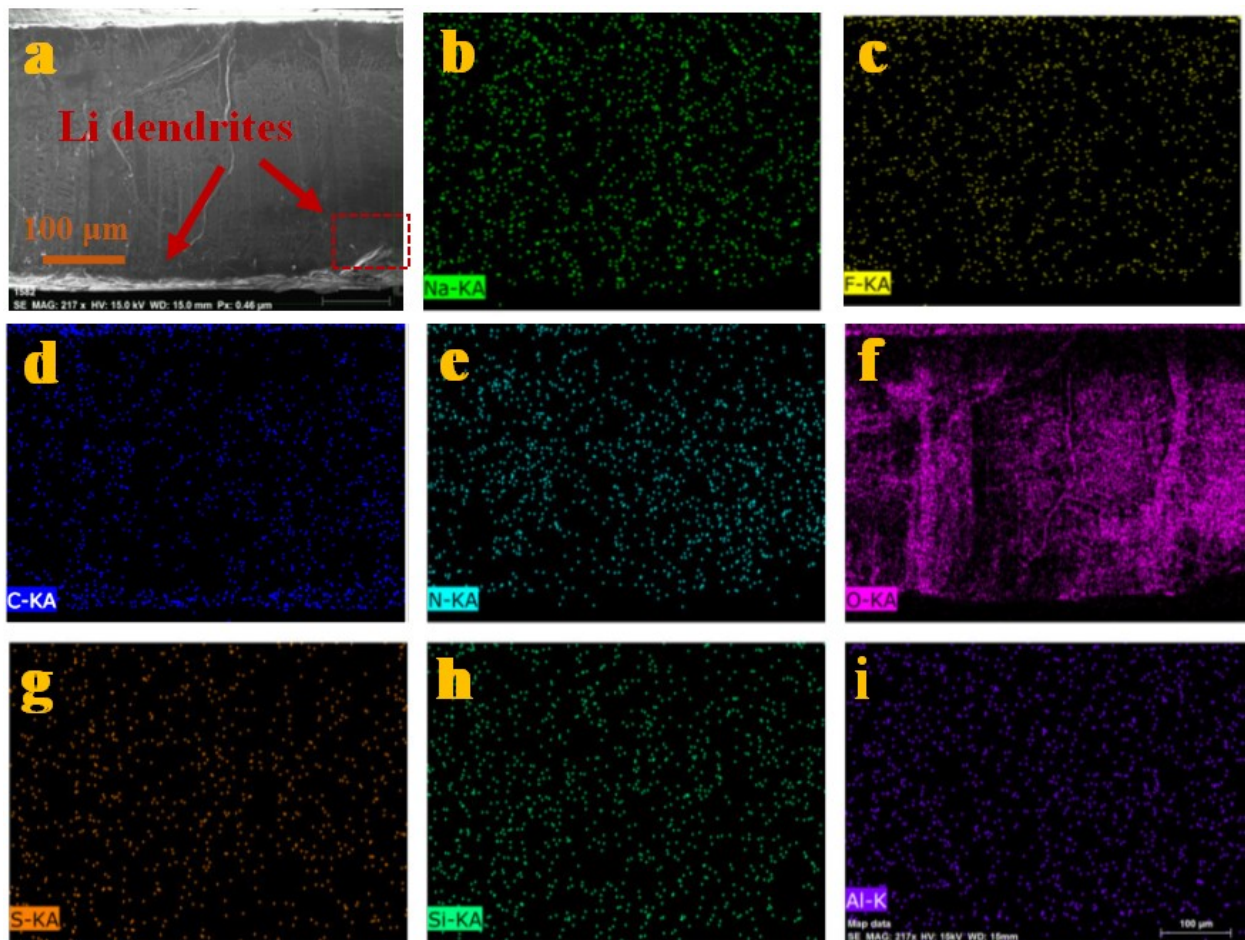


Fig. S24. Cross-sectional SEM and SEM-EDX mapping of YNa-CPE-10 after cycling performance using [Li|YNa-CPE|Li] cell at different current densities @60 °C (a) SEM. EDS mapping for (b) Na, (c) F, (d) C, (e) N, (f) O, (g) S, (h) Si, and (i) Al elements.

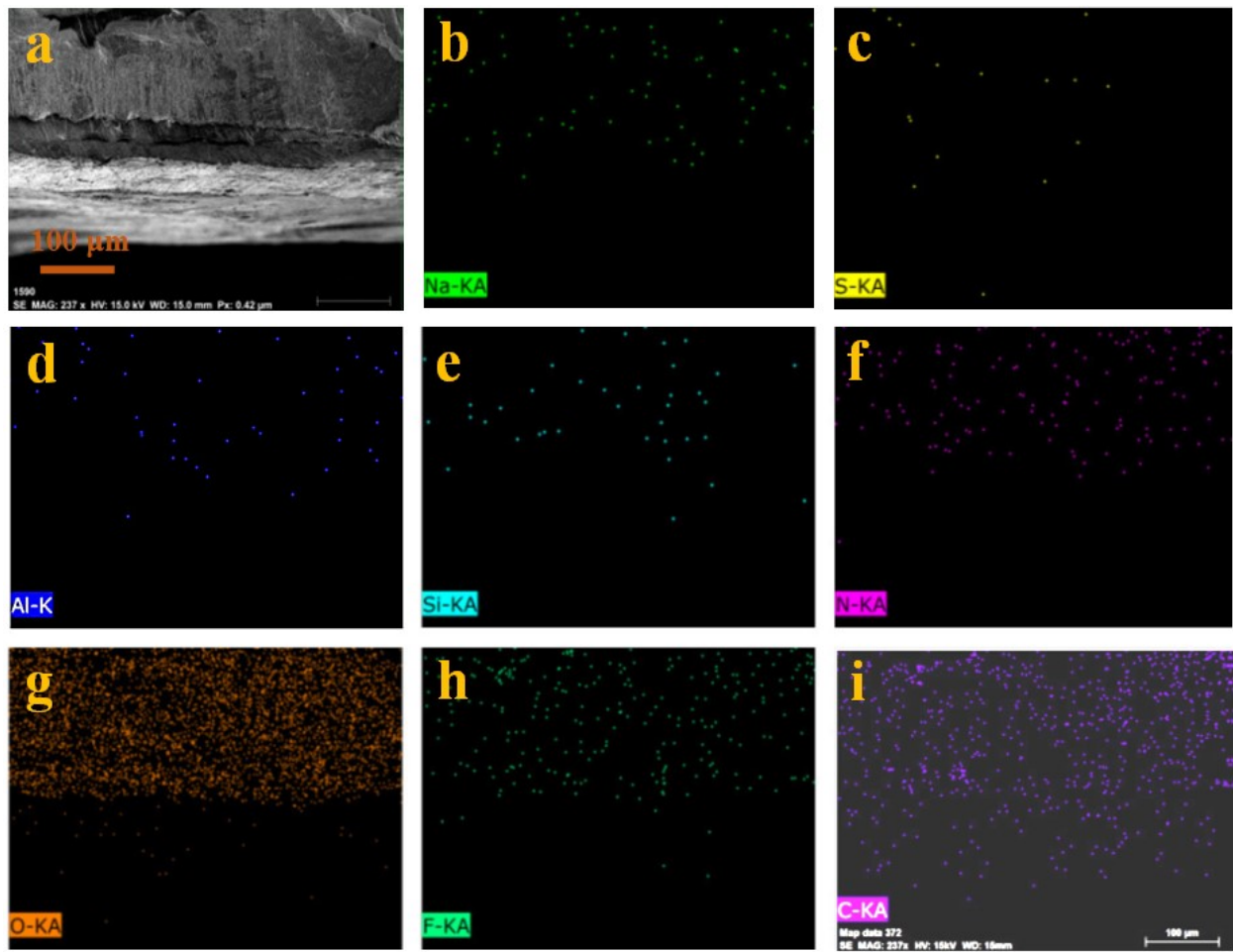


Fig. S25. Cross-sectional SEM and SEM-EDX mapping of YNa-CPE-35 after cycling performance using [Li|YNa-CPE|Li] cell at different current densities @60 °C (a) SEM. EDS mapping for (b) Na, (c) S, (d) Al, (e) Si, (f) N, (g) O, (h) F, and (i) C elements.

References:

- 1 Shalu, V. K. Singh and R. K. Singh, *J. Mater. Chem. C*, 2015, **3**, 7305–7318.
- 2 S. K. Chaurasia, A. L. Saroj, Shalu, V. K. Singh, A. K. Tripathi, A. K. Gupta, Y. L. Verma and R. K. Singh, *AIP Adv.*, 2015, **5**, 077178.
- 3 D. M. Pesko, Y. Jung, A. L. Hasan, M. A. Webb, G. W. Coates, T. F. Miller and N. P. Balsara, *Solid State Ionics*, 2016, **289**, 118–124.
- 4 W. Zhou, H. Gao and J. B. Goodenough, *Adv. Energy Mater.*, 2016, **6**, 1502130.
- 5 W. Li, S. Zhang, B. Wang, S. Gu, D. Xu, J. Wang, C. Chen and Z. Wen, *ACS Appl. Mater. Interfaces*, 2018, **10**, 23874–23882.
- 6 H. Jamal, F. Khan, S. Hyun, S. W. Min and J. H. Kim, *J. Mater. Chem. A*, 2016, **9**, 4126–4137.
- 7 J. Peng, L. N. Wu, J. X. Lin, C. G. Shi, J. J. Fan, L. Bin Chen, P. Dai, L. Huang, J. T. Li and S. G. Sun, *J. Mater. Chem. A*, 2019, **7**, 19565–19572.
- 8 L. Zhu, P. Zhu, Q. Fang, M. Jing, X. Shen and L. Yang, *Electrochim. Acta*, 2018, **292**, 718–726.
- 9 G. Wang, P. He and L. Z. Fan, *Adv. Funct. Mater.*, 2021, **31**, 2007198.
- 10 Z. Wan, D. Lei, W. Yang, C. Liu, K. Shi, X. Hao, L. Shen, W. Lv, B. Li, Q. H. Yang, F. Kang and Y. B. He, *Adv. Funct. Mater.*, 2019, **29**, 1805301.
- 11 L. Chen, Y. Li, S. P. Li, L. Z. Fan, C. W. Nan and J. B. Goodenough, *Nano Energy*, 2018, **46**, 176–184.